Anisotropy and boundary scattering in the lattice thermal conductivity of silicon nanomembranes

Z. Aksamija* and I. Knezevic†
Department of Electrical and Computer Engineering, University of Wisconsin–Madison, Madison, Wisconsin 53706, USA
(Received 11 May 2010; revised manuscript received 1 July 2010; published 27 July 2010)

We present a calculation of the full thermal conductivity tensor for (001), (111), and (011) surface orientations of the silicon-on-insulator (SOI) nanomembrane, based on solving the Boltzmann transport equation in the relaxation-time approximation with the full phonon dispersions, a momentum-dependent model for boundary scattering, as well as three-phonon and isotope scattering. The interplay between strong boundary scattering and the anisotropy of the phonon dispersions results in thermal conduction that strongly depends on the surface orientation and exhibits marked in-plane vs out-of-plane anisotropy, as well as slight in-plane anisotropy for the low-symmetry (011) SOI. In-plane thermal conductivity is highest along [100] on Si(011) and lowest in Si(001) due to the strong scattering of the highly anisotropic TA modes with (001) surfaces. The room-temperature in-plane conductivities in (011) and (001) nanomembranes with thicknesses around 10 nm differ by a factor of 2, and the ratio can be much higher at lower temperatures or in rougher samples. We discuss surface facet orientation as a means of tailoring thermal conduction in low-dimensional nanostructrures and address the role of out-of-plane thermal conductivities in predicting vertical phonon transport in superlattices.

DOI: 10.1103/PhysRevB.82.045319 PACS number(s): 63.20.K−, 63.22.−m, 65.80.−g, 66.70.−f

I. INTRODUCTION

Heat conduction in semiconductors is dominated by phonon transport.[1] Tetrahedrally bonded semiconductors have high lattice thermal conductivities (e.g., 148 W/mK for Si at room temperature[2]) thanks to the strong sp^3 bonds and relatively low atomic masses. High thermal conductivity is a great benefit in electronic applications, but makes these materials unsuitable for thermoelectric applications, where low thermal conductivity is needed.[3,4] Heat conduction in bulklike semiconductor samples is governed by three-phonon and isotope scattering while the effects of surface interactions become observable at low temperatures.[1,5]

In contrast, thermal transport in semiconductor nanostructures, such as silicon-on-insulator (SOI) membranes[6] and nanowires,[7,8] is strongly influenced by boundary scattering even at room temperature.[9,10] Recently, a decrease in thermal conductivity of nearly 2 orders of magnitude with respect to bulk was observed in rough silicon nanowires due to enhanced boundary scattering,[7,8,11] which has opened up possibilities of using silicon nanostructures as efficient thermoelectric materials.[12] Decreasing the feature size of nanostructures[13] and surface decoration[14] have also been shown to promote boundary scattering and lead to a thermal conductivity decrease. However, reducing the size of nanostructures below a few nanometers is technologically challenging while both size reduction and roughening penalize electronic properties through charge trapping and mobility lowering[15] and may overall be detrimental to the thermoelectric performance.[7,8] On the other hand, reduction in thermal conductivity is not always the goal: with transistor downscaling, hot-carrier and hot-phonon transport become exacerbated,[16] and increasing thermal conductivity in the nanoscale channel to facilitate cooling becomes very important in order to ensure stable and efficient electronic performance.[17,18] Therefore, it is important to seek additional means of tailoring—enhancing or reducing—the thermal conductivity in semiconductor nanostructures, such that extreme downscaling and chemical processing are supplanted and detriment to electronic transport is minimized.[9,19]

In this paper, we investigate the sensitivity of thermal conduction in thin SOI membranes to the surface crystalline orientation, boundary roughness features, and the direction of heat flow. We calculate the full thermal conductivity tensor in (001), (011), and (111) silicon nanomembranes with thicknesses ranging from 5 to 100 nm. The calculation employs the full phonon dispersion and the Boltzmann transport equation, including three-phonon and isotope scattering as well as a momentum-dependent boundary scattering model. We demonstrate that the interplay between strong boundary scattering in SOI membranes and the anisotropy in the phonon dispersions results in thermal conduction that strongly depends on the surface orientation and exhibits marked in-plane vs out-of-plane anisotropy, as well as some in-plane anisotropy for low-symmetry surface orientations. For all nanomembrane surface orientations, the thermal conductivity tensor has an out-of-plane eigenvector, corresponding to the minimal eigenvalue that represents the intrinsic out-of-plane thermal conductivity of the membrane. In-plane thermal conductivity is overall highest along the [100] direction on (011) SOI [there is a slight anisotropy of the in-plane conductivity on (011) SOI] while the lowest in-plane conductivity is observed in (001) SOI due to the very strong scattering of the highly anisotropic TA modes with (001) surfaces. The room-temperature in-plane conductivities in (011) and (001) nanomembranes with thicknesses around 10 nm differ by a factor of 2. This ratio can get much higher with increased prominence of boundary scattering, i.e., with lower temperatures, intentionally roughened surfaces, or in very thin samples. We conclude that, for applications that require good thermal conduction such as in digital electronics, heating will be minimized in SOI devices if the channel is oriented as [100]/(011). In contrast, for thermoelectric applications where low thermal conductivity is needed, the best starting points are likely to be nanostructures with as many {001}

facets as possible to promote the boundary scattering of TA modes, such as in etched rectangular [100] nanowires with (001) and (010) facets.

The paper is organized as follows: in Sec. II, we present the phonon transport model, discuss the calculation of the different scattering rates and elaborate on the momentum-dependent specularity parameter for the treatment of boundary scattering. In Sec. III, we present the eigenvectors and eigenvalues of the thermal conductivity tensor for SOI nanomembranes of different surface orientations, thicknesses, and roughnesses. We discuss the interplay between the full-dispersion anisotropy and boundary roughness and the consequences it has on the surface-orientation sensitivity of thermal conductivity. We conclude in Sec. IV with a brief summary and a few final remarks.

II. PHONON TRANSPORT MODEL

The simplest models of thermal conductivity—the Klemens-Callaway[20,21] and Holland models[22]—fail to capture the anisotropy of thermal conductivity[23,24] as they rely on the Debye approximation (linear and isotropic acoustic phonon dispersion) in conjunction with isotropic three-phonon and isotope scattering, as well as an empirical, momentum-independent specularity parameter to treat boundary scattering.[25,26] In this work, in order to capture the full anisotropy of lattice heat conduction, we calculate the thermal-conductivity tensor

$$\mathbf{K}^{\alpha\beta}(T) = k\sum_{\mathrm{j}}\sum_{\vec{q}}\left[\frac{\hbar\omega_{\mathrm{j}}(\vec{q})}{kT}\right]^2 \frac{e^{\hbar\omega_{\mathrm{j}}(\vec{q})/kT}}{[e^{\hbar\omega_{\mathrm{j}}(\vec{q})/kT}-1]^2} \times \tau_{\mathrm{j}}(q)v_{\mathrm{j}}^{\alpha}(\vec{q})v_{\mathrm{j}}^{\beta}(\vec{q}), \quad (1)$$

where $v_{\mathrm{j}}^{\alpha}(\vec{q})$ and $\omega_{\mathrm{j}}(\vec{q})$ are the αth component of the phonon velocity vector and the frequency in branch j, respectively, while k is the Boltzmann constant, and T is the temperature. We calculate the full phonon dispersion from the adiabatic bond charge model[27,28] that accurately captures the phonon dispersions in all directions.[29] Bulk dispersions give an accurate description of phonon states in SOI as thin as 5 nm.[30–32]

In the calculation of the relaxation time $\tau_{\mathrm{j}}(\vec{q})$ for a phonon in mode j and with wave vector $\vec{q}$, we consider normal (N) and umklapp (U) three-phonon scattering, isotope scattering (I), and boundary surface-roughness (B) scattering with branch- and momentum-dependent relaxation times $\tau_{\mathrm{j,N}}(\vec{q})$, $\tau_{\mathrm{j,U}}(\vec{q})$, $\tau_{\mathrm{j,I}}(\vec{q})$, and $\tau_{\mathrm{j,B}}(\vec{q})$, respectively. The total relaxation time $\tau_{\mathrm{j}}(\vec{q})$ is given by

$$\frac{1}{\tau_{\mathrm{j}}(\vec{q})} = \frac{1}{\tau_{\mathrm{j,N}}(\vec{q})} + \frac{1}{\tau_{\mathrm{j,U}}(\vec{q})} + \frac{1}{\tau_{\mathrm{j,I}}(\vec{q})} + \frac{1}{\tau_{\mathrm{j,B}}(\vec{q})}. \quad (2)$$

A. Three-phonon and isotope scattering

With the exception of $1/\tau_{\mathrm{j,B}}$, the scattering rates do not depend on the phonon momentum direction explicitly but rather on its energy and are thus constant on energy isosurfaces. The dependence of N and U relaxation times on the phonon energy and lattice temperature can be expressed through

$$\frac{1}{\tau_{\mathrm{j,N/U}}^{\mathrm{LA/TA}}(\omega)} = A_{\mathrm{N/U}}^{\mathrm{TA/LA}}\omega_{\mathrm{j}}^{n}g(T), \quad (3)$$

where $n=2$ for normal scattering and $n=4$ for umklapp scattering.[33] This model, based on *ab initio* calculations, gives a natural crossover between normal scattering, dominant among low-energy phonons, and umklapp scattering, dominant among higher-energy phonons.[33] The temperature function is given by $g(T)=T[1-\exp(-3T/\Theta_D)]$ with $\Theta_D=645$ K being the Debye temperature of silicon.[34] The constants $A_{\mathrm{N/U}}^{\mathrm{TA/LA}}$ are dependent on the polarization of the phonon branch. Based on *ab initio* calculations,[33] their values are $A_{\mathrm{N}}^{\mathrm{TA}}=253322$ $(\mathrm{meV}^2\ \mathrm{K\ s})^{-1}$ for the transverse acoustic modes and $A_{\mathrm{N}}^{\mathrm{LA}}=163921$ $(\mathrm{meV}^2\ \mathrm{K\ s})^{-1}$ for the longitudinal acoustic mode. For umklapp scattering, the constants are $A_{\mathrm{U}}^{\mathrm{TA}}=2012$ $(\mathrm{meV}^2\ \mathrm{K\ s})^{-1}$ and $A_{\mathrm{U}}^{\mathrm{LA}}=507$ $(\mathrm{meV}^4\ \mathrm{K\ s})^{-1}$.

Isotope scattering has no temperature dependence, and the energy dependence of the isotope scattering rate is calculated from[35,36]

$$\frac{1}{\tau_{\mathrm{I}}(\omega)} = \frac{\pi V_0}{6}\Gamma_{\mathrm{Si}}\omega^2\mathrm{VDOS}(\omega), \quad (4)$$

where V_0 is the volume per atom and $\mathrm{VDOS}(\omega)$ is the vibrational density of states calculated from the full phonon dispersion using the method of Gilat and Raubenheimer[37] [see Fig. 2(b)]. $\Gamma_{\mathrm{Si}}=\Sigma_i f_i(1-m_i/\bar{m})^2$, where f_i is the natural abundance of isotope i with mass m_i, and the average mass is $\bar{m}=\Sigma_i f_i m_i$. The value of Γ_{Si} is 2.0×10^{-4}.[34]

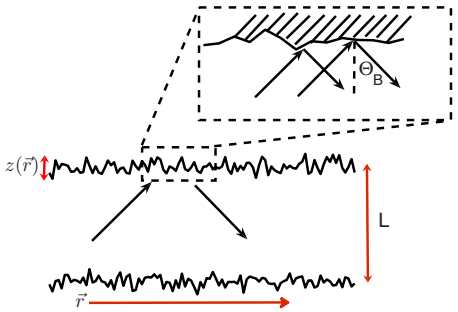

FIG. 1. (Color online) Schematic of a silicon nanomembrane of thickness L, showing a lattice wave scattering from the rough boundary. The phases of the waves reflected from different points on the boundary differ by amounts that depend on the local surface-roughness height $z(\vec{r})$ and the angle Θ_B between the phonon momentum $\vec{q}$ and the boundary surface normal of the idealized smooth surface.

B. Momentum-dependent specularity parameter for boundary roughness scattering

In order to describe boundary roughness scattering, we consider a thin silicon-on-insulator layer in the xy plane. Each boundary is assumed to be rough with a deviation from an ideally smooth surface characterized by surface-roughness height $z(\vec{r})$ at in-plane position $\vec{r}=(x,y)$ (see Fig. 1). We will

assume that z is a random variable with a Gaussian distribution so that $\langle z\rangle=0$ and $\langle z^2\rangle=\Delta^2$, where Δ is the rms height of the surface roughness.[38]

When a plane lattice wave with wave vector $\vec{q}$ strikes the rough surface, the reflected wave contains a specular component and a diffuse component.[39] The magnitude and isotropy of the diffusely scattered wave depend greatly on the boundary roughness correlation length $\lambda_{B,corr}$: in the case of highly correlated surfaces, where the correlation length is comparable to or exceeds the phonon wavelength, the diffuse part is strongly anisotropic and peaks around the direction of the specularly reflected wave, merging with it and effectively making the surface appear smoother.[40] For lattice thermal transport, the worst-case scenario is that of an effectively uncorrelated surface, for which the correlation length is much smaller than the typical wavelength ($\lambda_{B,corr}\ll\lambda$) and the diffusely scattered wave is nearly isotropic and does not contribute to the current flow. This approximation is good for an unintentionally roughened Si surface[41] and long-wavelength acoustic phonons in silicon, and we will assume it henceforth.

In the case of weak correlation, surface-roughness scattering can be effectively characterized through a momentum-dependent specularity parameter[40] $p(\vec{q})=\exp(-\langle\phi^2\rangle)$, where $\phi(\vec{q},\vec{r})=2\vec{q}\cdot\hat{s}z(\vec{r})=2qz(\vec{r})\cos\Theta_B$ is the phase difference between the incoming wave and the outgoing specularly reflected wave at point $\vec{r}$ where the surface normal unit vector is $\hat{s}$ (see Fig. 1). [This expression for $\phi(\vec{q},\vec{r})$ assumes that the boundary is between silicon and an acoustically softer medium (i.e., one with a lower acoustic impedance ρv_s, a product of density and average sound velocity) such as between silicon and amorphous silicon dioxide;[42] in the case of reflection from an acoustically harder medium, an additional π would be present in ϕ.] The distribution of ϕ over the xy plane follows that of z, so $\langle\phi^2\rangle=(2q\cos\Theta_B)^2\langle z^2\rangle=4q^2\Delta^2\cos^2\Theta_B$, and finally

$$p(\vec{q})=\exp(-4q^2\Delta^2\cos^2\Theta_B). \tag{5}$$

Figure 2(a) depicts the temperature variation in the average specularity parameter per phonon branch, $\bar{p}_j$, for the LA (solid), TA1 (dashed), and TA2 (dashed-dotted) branches, and with the surface-roughness rms heights of $\Delta=0.1$, 0.5, and 1.5 nm. $\bar{p}_j$ is a weighted average over all phonon momenta on a given branch

$$\bar{p}_j=\frac{\int p(\vec{q})N_0[\omega_j(\vec{q})]d^3\vec{q}}{\int N_0[\omega_j(\vec{q})]d^3\vec{q}}, \tag{6}$$

where N_0 is the equilibrium Bose-Einstein phonon distribution function. $\bar{p}_j$, an ensemble quantity, depends on temperature and Δ.

For each branch, one notices a specular-to-diffuse transition, connected to the increasing abundance of large-q phonons that scatter diffusely with increasing temperatures. The transition temperature range depends on the phonon branch and Δ, the rms of surface-roughness fluctuations. Phonon dispersions and density of states for LA and TA branches are depicted in Fig. 2(b). [For completeness, LO and the two TO branches are depicted as well but their contribution to thermal conductivity is neglected since their velocities are small and they are typically unpopulated at temperatures of interest here (up to 400 K).] We see that TA modes scatter more diffusely, i.e., their specular-to-diffuse transition range occurs at lower temperatures than that of LA modes. The reason is the following: large-q (near-Brillouin-zone-edge) TA modes, that scatter most from boundaries due to their large q [see Eq. (5)], flatten fairly low in energy [Fig. 2(b)], thus having a large VDOS and being abundant down to low temperatures, which together result in fairly strong boundary scattering on average. In contrast, LA modes near the Brillouin-zone edge (those that scatter most diffusely) come with steeper dispersions (lower VDOS) and have higher energies, so higher temperatures are needed to populate them. Therefore, up to high temperatures, LA phonons on average scatter more specularly (view a given surface as smoother) than TA phonons.

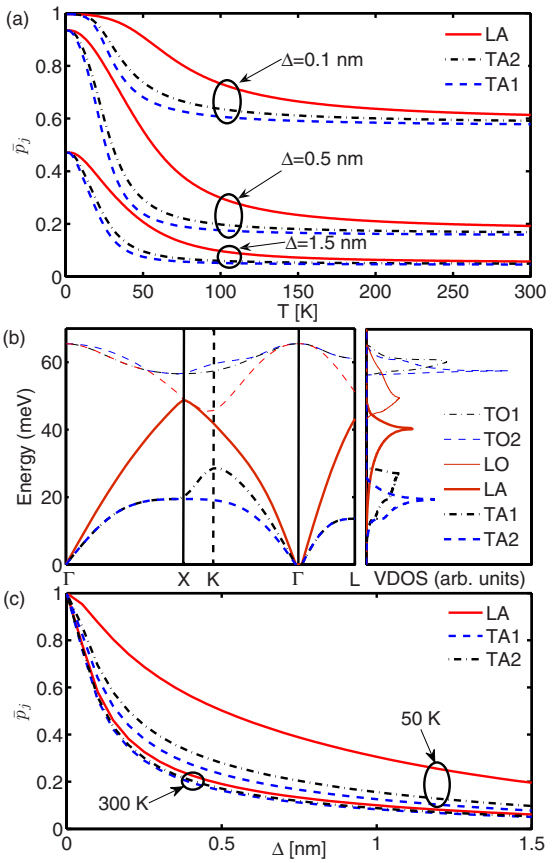

FIG. 2. (Color online) Average specularity parameter for LA (solid), TA1 (dashed), and TA2 (dashed-dotted) phonon branches. (a) Temperature variation in the average specularity parameter per phonon branch with surface-roughness rms heights of $\Delta=0.1$, 0.5, and 1.5 nm. (b) Phonon dispersions and density of states for the acoustic branches. For completeness, optical-mode dispersions are also depicted. (c) Variation in the average specularity parameter with the rms roughness Δ at 300 K (thick curves) and 50 K (thin curves).

As one approaches room temperature, the simple concept of a single, momentum-independent specularity parameter

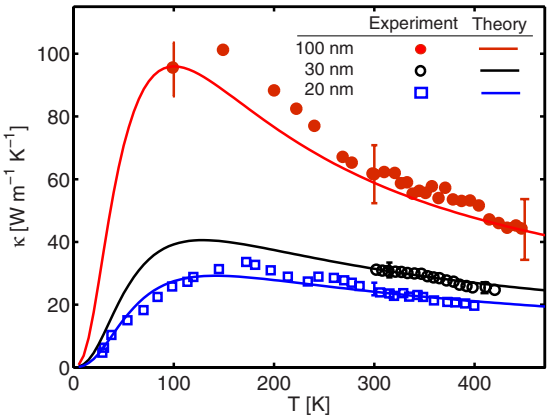

FIG. 3. (Color online) Lattice thermal conductivity of 100 nm (filled circles), 30 nm (open circles), and 20 nm (squares) thick SOI, according to the measurements of Refs. 46 and 47. The curves present our calculations with $\Delta=0.35$ nm for 100 nm SOI, $\Delta=0.4$ nm for 30, and $\Delta=0.45$ nm for 20 nm SOI, in very good agreement with experiment. Thermal conductivity is lower by almost an order of magnitude than the room-temperature bulk value of 148 W/mK, owing primarily to boundary scattering at the rough Si/SiO_2 interfaces.

that is often employed in calculations[43] becomes better justified. Figure 2(c) presents how the averaged specularity parameter relates to the rms height of surface roughness. At low temperatures, the full effect of the phonon dispersion on specularity is obvious, and LA modes have a markedly higher specularity parameter than TA modes. At room temperature, as large-q LA phonons become more abundant, a single specularity parameter is adequate to use.

The discussion above holds for a single Si/SiO_2 boundary. In the case of SOI, scattering occurs between opposing surface boundaries that can be considered mutually uncorrelated because they are processed separately.[41] We assume an effective average Δ, and hence the same specularity parameter, Eq. (5), for both boundaries. Bouncing between two boundaries separated by membrane thickness L, phonon momentum will have a lifetime proportional to the time it takes the phonon to cross the membrane,[39,44,45]

$$\tau_{j,B}(\vec{q}) = \left[\frac{1+p(\vec{q})}{1-p(\vec{q})}\right]\frac{L}{v_{j,\perp}(\vec{q})}, \tag{7}$$

where $v_{j,\perp}(\vec{q})=v_j(\vec{q})\cdot\hat{s}$ is the velocity component normal to the surface. Clearly, phonons with the velocity directed into the surface will have the shortest lifetime.

III. THERMAL-CONDUCTIVITY TENSOR IN THIN SILICON MEMBRANES

From the full thermal conductivity tensor Eq. (1), we can compute thermal conductivity along any direction as $\kappa=\mathbf{K}_{\alpha\beta}\hat{n}^{\alpha}\hat{n}^{\beta}$ with $\hat{n}$ being the unit vector along the direction. In Fig. 3, we compare the directional in-plane thermal conductivity κ with experimental values of 20, 30, and 100 nm SOI.[46,47] The surface orientation was assumed to be (001), and the best agreement was obtained with roughness rms height $\Delta=0.3$ nm for the 100 nm SOI, $\Delta=0.4$ nm for the 30 nm, and $\Delta=0.45$ nm for the 20 nm SOI. The computed values of κ are in very good agreement with the measurements[46,47] on thin SOI (Fig. 3) at both high and low temperatures.

We calculated the full thermal conductivity tensor, Eq. (1), for SOI nanomembranes with (001), (011), and (111) surface orientations and a variety of surface-roughness rms heights and membrane thicknesses (5–100 nm). For every SOI surface orientation, the full thermal conductivity tensor, Eq. (1), has three eigenvector/eigenvalue pairs with the eigenvectors independent of temperature. In Fig. 4(a), we compare the eigenvalues of the room-temperature thermal conductivity tensors for 20 nm SOI with $\Delta=0.45$ nm (the same value as in Fig. 3) but with different surface orientations: (001), (011), and (111). As intuitively expected, there is a strong in-plane vs out-of-plane anisotropy in heat conduction for all surface orientations with one eigenvector always pointing out of plane and the corresponding thermal-conductivity eigenvalues being considerably lower than in-plane ones due to stronger boundary scattering.[24,48,49]

An important feature of Fig. 4(a) is that in-plane thermal conductivity eigenvalues for different SOI surface orientations differ significantly from one another. This behavior can be explained based on the acoustic phonon dispersions alone, as the contribution of optical phonons to thermal conductivity in silicon is negligible, owing to their high energies (and thus low population at temperatures of interest here) and low group velocities [see Fig. 2(b)]. The sensitivity of thermal conductivity to the surface orientation is intimately connected to the full phonon dispersions, and best depicted by looking at the TA [Fig. 4(b)] and LA [Fig. 4(c)] energy isosurfaces because phonon velocity at a given $\vec{q}$ is perpendicular to the isosurface on which that $\vec{q}$ lies. The TA constant-energy surfaces are boxlike [Fig. 4(b)] with box faces perpendicular to ⟨001⟩ directions. As a result, TA phonon velocities are mostly directed along ⟨001⟩ directions, and therefore TA modes scatter very strongly from the boundaries in (001) SOI [see Eq. (7)]. LA phonon energy isosurfaces are nearly isotropic (spherical) for small energies but at larger energies they mimic the shape of the Brillouin zone [Fig. 4(c)] with hexagonal ⟨111⟩ and square ⟨001⟩ faces. Therefore, large-q LA phonons have velocities directed preferentially along ⟨111⟩ and scatter very strongly from Si(111) boundaries with a small proportion of phonons having velocities along ⟨001⟩ and scattering strongly from Si(001) boundaries. It is also important to note that the velocities of LA modes at large q are much larger in magnitude than those of TA modes (see Fig. 2), and therefore LA modes scatter with higher rates than TA phonons from their respective preferred boundaries. That is why, in spite of having both TA branches and a portion of the LA branch scatter preferentially from Si(001), the thermal conductivity in Si(001) is not dramatically lower than that of Si(111).

In contrast to Si(001) and Si(111), none of the modes couple very strongly to the low-symmetry Si(011), so in-plane thermal conductivity is highest on this SOI orientation. The in-plane thermal conductivity on Si(011) also displays a slight anisotropy: thermal-conductivity eigenvalue along [100] on Si(011) is higher than that along [011] on Si(011),

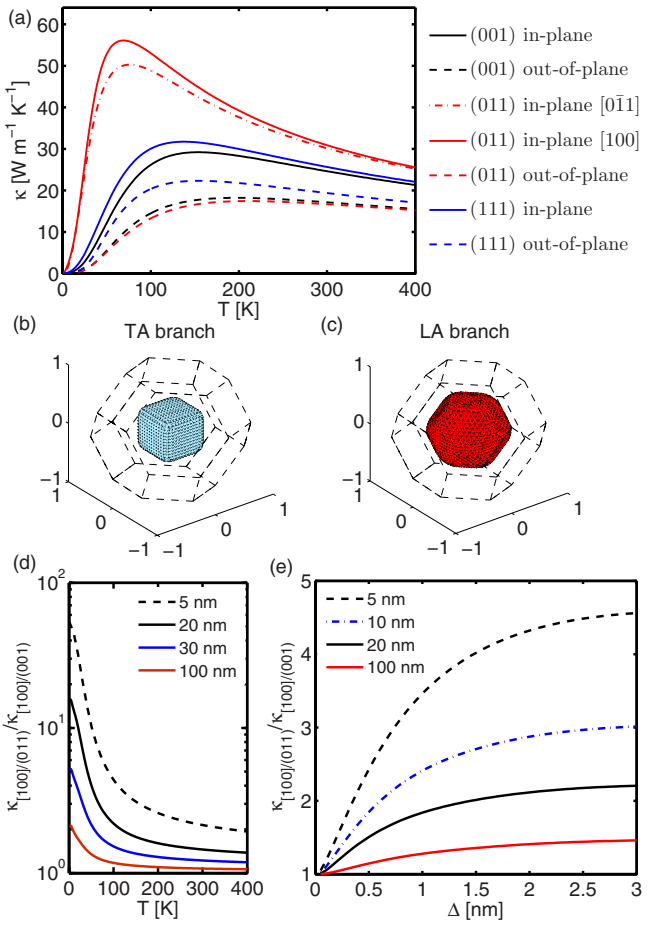

FIG. 4. (Color online) Lattice thermal conduction in thin SOI membranes. (a) Eigenvalues of the thermal conductivity tensor (1) for a 20-nm-thick SOI with rms surface roughness $\Delta=0.45$ nm. Maximal in-plane thermal conductivity eigenvalue is along [100] on (011) SOI and it is minimal on (001) SOI due to the very strong scattering of TA modes from (001) boundaries, as described in the text. [(b) and (c)] Energy isosurfaces for (c) TA and (d) LA modes in silicon (dashed lines denote the Brillouin-zone shape). The TA constant-energy surfaces are boxlike with box faces perpendicular to ⟨001⟩ directions. The LA mode energy isosurfaces have faces perpendicular to ⟨111⟩ and ⟨001⟩ directions. [(d) and (e)] Ratio of the highest to the lowest in-plane thermal conductivity, $\kappa_{[100]/(011)}/\kappa_{[100]/(001)}$, for SOI with thicknesses in the 5–100 nm range, as a function of (d) temperature (surface-roughness rms height is 0.4 nm) and (e) rms roughness height (at room temperature).

again owing to phonon focusing along [100].

The full phonon dispersions play a critical role in revealing the sensitivity of the thermal conductivity to the surface orientation and the direction of heat flow. Namely, if instead of the full dispersions we used the isotropic Debye model (with mode-dependent velocities but the phonon velocity and momentum colinear and independent of direction), we would still capture the difference between the in-plane and out-of-plane thermal conductivities because of boundary scattering, but there would be no dependence on the surface orientation or the direction of heat flow.

Overall, in-plane thermal conductivity is maximal along [100] on (011) SOI and minimal on (001) SOI. The ratio of the highest to the lowest in-plane thermal conductivity, $\kappa_{[100]/(011)}/\kappa_{[100]/(001)}$, is presented in Fig. 4(d) as a function of temperature for 5, 20, 30, and 100 nm thin SOI. All are assumed to have $\Delta=0.4$ nm, a value that represents unintentional roughening due to standard silicon processing well.[41] At low temperatures, where three-phonon scattering is weak, scattering due to boundaries becomes the most pronounced mechanism; the different $\kappa_{[100]/(011)}/\kappa_{[100]/(001)}$ ratios for different thicknesses in the low-temperature limit fully reveal the different strength of phonon scattering from differently oriented boundaries. In Fig. 4(e), we see how the ratio $\kappa_{[100]/(011)}/\kappa_{[100]/(001)}$ at room temperature depends on the SOI thickness and rms roughness Δ. Even without intentional roughening ($\Delta\sim0.5$ nm), samples of thicknesses around 10 nm have twice the thermal conductivity on Si(011) than they do on Si(001); with roughening, thermal conductivity in Si(001) drops faster as it is a preferred scattering boundary for TA phonons.

We conclude that for electronic applications of SOI where high thermal conductivity is desirable,[9,17,18] heating will be minimized in a device channel oriented as [100]/(011). The rougher the surface, the more important it becomes to choose Si(011) over Si(001) for high thermal conductivity. In contrast, if low thermal conductivity is needed in a nanostructure, roughening will be most efficient on Si(001) nanomembranes that ensure strong boundary scattering.

IV. CONCLUSION

In summary, we have calculated the full thermal conductivity tensor in (001), (011), and (111) SOI nanomembranes based on solving the Boltzmann transport equation while accounting for the full phonon dispersion, momentum-dependent boundary scattering, as well as three-phonon and isotope scattering. In-plane thermal conductivity is minimal on (001) Si nanomembranes, due to the strong coupling of TA modes to (001) surfaces. Highest in-plane conductivity is achieved along [100] on the low-symmetry (011) SOI. Therefore, for applications requiring efficient passive cooling (i.e., high thermal conductivity), such as in digital electronic circuits, [100]/(011) should offer twice the thermal conductivity of Si(001) at room temperature even in relatively thick (~10 nm) nanomembranes. The rougher the samples, the more pronounced the surface-orientation dependence of the in-plane thermal conductivity becomes.

Overall, the strong interplay between the phonon dispersion anisotropy and boundary scattering enables one to have the surface facet orientation as an additional degree of control over thermal conduction in nanostructures. A natural extension of this conclusion pertains to the use of nanowires in thermoelectric applications. In rectangular or square wires, which can be fabricated by lithography and etching from Si nanomembranes,[50] thermal conductivity is expected to be lowest for [100] wires with (001) and (010) surface facets. Therefore, intentional roughening, feature size reduction, and surface decoration of nanowires, often pursued in thermoelectric applications, are likely to bring the most detriment to thermal conductivity if applied to these wires. Thermal conductivity will likely be lower in square top-down nanowires

with {001} surface facets than in their self-assembled counterparts with nearly circular or hexagonal cross-sections, in which the multifaceted nature of the surface results in less boundary scattering overall.

Lastly, out-of-plane thermal conductivity of superlattice stacks has been of interest for sometime, but we are far from a full understanding.[43,48,51,52] The technique presented here does not localize the phonon in the membrane's vertical direction but rather treats boundary scattering as yet another scattering mechanism (in contrast to real-space techniques such as Monte Carlo[53,54] or Discrete Ordinate[48,55] methods, which have real-space boundaries). Therefore, heat flow in the direction normal to the surface is not precluded and the method presented here can be readily extended to calculate the intrinsic out-of-plane conductivity of individual layers in a superlattice, with proper boundary conditions to account for the thermal impedance mismatch between adjacent layers.

ACKNOWLEDGMENTS

This work has been supported by the Computing Innovation Fellows Project (NSF Award No. 0937060 to the Computing Research Association, subaward CIF-146 to the University of Wisconsin) and by the AFOSR YIP program (Award No. FA9550-09-1-0230). The authors thank M. G. Lagally for comments on the manuscript.

*aksamija@wisc.edu
†knezevic@engr.wisc.edu

[1] G. P. Srivastava, *The Physics of Phonons* (Taylor & Francis, New York, NY, 1990).
[2] C. J. Glassbrenner and G. A. Slack, Phys. Rev. **134**, A1058 (1964).
[3] F. J. DiSalvo, Science **285**, 703 (1999).
[4] A. Majumdar, Nat. Nanotechnol. **4**, 214 (2009).
[5] *Thermal Conductivity*, Physics of Solids and Liquids, edited by T. M. Tritt (Springer, New York, NY, 2004).
[6] M. Asheghi, Y. K. Leung, S. S. Wong, and K. E. Goodson, Appl. Phys. Lett. **71**, 1798 (1997).
[7] A. I. Boukai, Y. Bunimovich, J. Tahir-Kheli, J. Yu, W. A. Goddard III, and J. R. Heath, Nature (London) **451**, 168 (2008).
[8] A. Hochbaum, R. Chen, R. Delgado, W. Liang, E. Garnett, M. Najarian, A. Majumdar, and P. Yang, Nature (London) **451**, 163 (2008).
[9] D. G. Cahill, W. K. Ford, K. E. Goodson, G. D. Mahan, A. Majumdar, H. J. Maris, R. Merlin, and S. R. Phillipot, J. Appl. Phys. **93**, 793 (2003).
[10] R. Chen, A. I. Hochbaum, P. Murphy, J. Moore, P. Yang, and A. Majumdar, Phys. Rev. Lett. **101**, 105501 (2008).
[11] P. Martin, Z. Aksamija, E. Pop, and U. Ravaioli, Phys. Rev. Lett. **102**, 125503 (2009).
[12] I. Chowdhury, R. Prasher, K. Lofgreen, G. Chrysler, S. Narasimhan, R. Mahajan, D. Koester, R. Alley, and R. Venkatasubramanian, Nat. Nanotechnol. **4**, 235 (2009).
[13] D. Donadio and G. Galli, Phys. Rev. Lett. **102**, 195901 (2009).
[14] T. Markussen, A.-P. Jauho, and M. Brandbyge, Phys. Rev. Lett. **103**, 055502 (2009).
[15] E. B. Ramayya, D. Vasileska, S. M. Goodnick, and I. Knezevic, J. Appl. Phys. **104**, 063711 (2008).
[16] E. Pop, S. Sinha, and K. Goodson, Proc. IEEE **94**, 1587 (2006).
[17] K. Raleva, D. Vasileska, S. M. Goodnick, and M. Nedjalkov, IEEE Trans. Electron Devices **55**, 1306 (2008).
[18] E. Pop, Nano Res. **3**, 147 (2010).
[19] A. A. Balandin, J. Nanosci. Nanotechnol. **5**, 1015 (2005).
[20] P. Klemens, *Solid state physics* (Academic Press, NY, 1958).
[21] J. Callaway, Phys. Rev. **113**, 1046 (1959).
[22] M. G. Holland, Phys. Rev. **132**, 2461 (1963).
[23] N. Mingo, L. Yang, D. Li, and A. Majumdar, Nano Lett. **3**, 1713 (2003).
[24] D. Baillis and J. Randrainalisoa, Int. J. Heat Mass Transfer **52**, 2516 (2009).
[25] G. Chen, J. Heat Transfer **119**, 220 (1997).
[26] P. Chantrenne, J. L. Barrat, X. Blase, and J. D. Gale, J. Appl. Phys. **97**, 104318 (2005).
[27] W. Weber, Phys. Rev. Lett. **33**, 371 (1974).
[28] W. Weber, Phys. Rev. B **15**, 4789 (1977).
[29] D. Strauch and B. Dorner, J. Phys. Condens. Matter **2**, 1457 (1990).
[30] R. Prasher, T. Tong, and A. Majumdar, Nano Lett. **8**, 99 (2008).
[31] C. Dames and G. Chen, J. Appl. Phys. **95**, 682 (2004).
[32] N. Mingo, Phys. Rev. B **68**, 113308 (2003).
[33] A. Ward and D. A. Broido, Phys. Rev. B **81**, 085205 (2010).
[34] D. T. Morelli, J. P. Heremans, and G. A. Slack, Phys. Rev. B **66**, 195304 (2002).
[35] S.-I. Tamura, Phys. Rev. B **27**, 858 (1983).
[36] D. A. Broido, A. Ward, and N. Mingo, Phys. Rev. B **72**, 014308 (2005).
[37] G. Gilat and L. J. Raubenheimer, Phys. Rev. **144**, 390 (1966).
[38] S. M. Goodnick, D. K. Ferry, C. W. Wilmsen, Z. Liliental, D. Fathy, and O. L. Krivanek, Phys. Rev. B **32**, 8171 (1985).
[39] J. Ziman, *Electrons and Phonons: The Theory of Transport Phenomena in Solids* (Oxford University Press, New York, 1960).
[40] S. B. Soffer, J. Appl. Phys. **38**, 1710 (1967).
[41] F. Chen, E. B. Ramayya, C. Euaruksakul, F. J. Himpsel, G. K. Celler, B. J. Ding, I. Knezevic, and M. G. Lagally, ACS Nano **4**, 2466 (2010).
[42] L. E. Kinsler, A. R. Fry, A. B. Coppens, and J. V. Sanders, *Fundamentals of Acoustics* (Wiley, New York, 2000).
[43] G. Chen, Phys. Rev. B **57**, 14958 (1998).
[44] A. Balandin and K. L. Wang, Phys. Rev. B **58**, 1544 (1998).
[45] J. S. Heron, T. Fournier, N. Mingo, and O. Bourgeois, Nano Lett. **9**, 1861 (2009).
[46] W. Liu and M. Asheghi, J. Heat Transfer **128**, 75 (2006).
[47] W. Liu and M. Asheghi, J. Appl. Phys. **98**, 123523 (2005).
[48] D. Terris, K. Joulain, D. Lemonnier, D. Lacroix, and P. Chantrenne, Int. J. Therm. Sci. **48**, 1467 (2009).
[49] C. J. Gomes, M. Madrid, J. V. Goicochea, and C. H. Amon, J. Heat Transfer **128**, 1114 (2006).
[50] M. Huang, C. S. Ritz, B. Novakovic, D. Yu, Y. Zhang, F. Flack,

D. E. Savage, P. G. Evans, I. Knezevic, F. Liu, and M. G. Lagally, ACS Nano **3**, 721 (2009).
[51] Y. K. Koh, Y. Cao, D. G. Cahill, and D. Jena, Adv. Funct. Mater. **19**, 610 (2009).
[52] G. Pernot, M. Stoffel, I. Savic, F. Pezzoli, P. Chen, G. Savelli, A. Jacquot, J. Schumann, U. Denker, I. Mönch, C. Deneke, O. G. Schmidt, J. M. Rampnoux, S. Wang, M. Plissonnier, A. Rastelli, S. Dilhaire, and N. Mingo, Nature Mater. **9**, 491 (2010).
[53] D. Lacroix, K. Joulain, and D. Lemonnier, Phys. Rev. B **72**, 064305 (2005).
[54] S. Mazumder and A. Majumdar, J. Heat Transfer **123**, 749 (2001).
[55] D. Terris, K. Joulain, D. Lemonnier, and D. Lacroix, J. Appl. Phys. **105**, 073516 (2009).